Hot Dense Capsule-Implosion Cores Produced by *Z*-Pinch Dynamic Hohlraum Radiation

J. E. Bailey,[1] G. A. Chandler,[1] S. A. Slutz,[1] I. Golovkin,[2] P.W. Lake,[1] J. J. MacFarlane,[2] R. C. Mancini,[3] T. J. Burris-Mog,[3] G. Cooper,[4] R. J. Leeper,[1] T. A. Mehlhorn,[1] T. C. Moore,[5] T. J. Nash,[1] D. S. Nielsen,[5] C. L. Ruiz,[1] D. G. Schroen,[6] and W. A. Varnum[7]

[1]*Sandia National Laboratories, Albuquerque, New Mexico 87185-1196, USA*
[2]*Prism Computational Sciences, Madison, Wisconsin 53703, USA*
[3]*Department of Physics, University of Nevada, Reno, Nevada 89557, USA*
[4]*University of New Mexico, Albuquerque, New Mexico 87131, USA*
[5]*K-tech Corporation, Albuquerque, New Mexico 87185, USA*
[6]*Schafer Corp., Livermore, California, 94550, USA*
[7]*Comforce Technical Services Inc., Albuquerque, New Mexico, 87185, USA*

(Received 21 May 2003; published 26 February 2004)

Hot dense capsule implosions driven by *Z*-pinch x rays have been measured using a ~220 eV dynamic hohlraum to implode 1.7–2.1 mm diameter gas-filled CH capsules. The capsules absorbed up to ~20 kJ of x rays. Argon tracer atom spectra were used to measure the $T_e \sim 1$ keV electron temperature and the $n_e \sim 1$–4×10^{23} cm^{-3} electron density. Spectra from multiple directions provide core symmetry estimates. Computer simulations agree well with the peak emission values of T_e, n_e, and symmetry, indicating reasonable understanding of the hohlraum and implosion physics.

DOI: 10.1103/PhysRevLett.92.085002 PACS numbers: 52.58.Lq, 52.57.Fg, 52.70.La

Implosion of spherical capsules by x rays contained in an enclosure known as a hohlraum is a promising approach for achieving inertial confinement fusion (ICF) [1]. One method for generating the required high energy density x rays is the *Z*-pinch dynamic hohlraum (ZPDH) [2–4]. Accelerating an annular high-atomic-number *Z*-pinch plasma onto a low-atomic-number low-density cylindrical foam creates this type of hohlraum. The *Z*-pinch plasma impact onto the foam launches a radiating shock that propagates toward the cylinder axis and heats the hohlraum. The *Z*-pinch plasma traps the radiation, improving the symmetry for driving capsule implosions at the center of the hohlraum. An overview of recent progress, leading to the first hot dense implosions produced using *Z*-pinch radiation, was provided in [5]. This Letter describes x-ray spectroscopy measurements of the implosion core electron temperature (T_e), electron density (n_e), areal density (ρr), and symmetry.

ICF requires highly symmetric capsule implosions. Absorption of 150 kJ of x-ray energy in a shaped pulse with $\sim(1-3)\%$ symmetry is estimated to be sufficient for ignition [1]. The appeal of the ZPDH approach is efficient generation and delivery of x rays to the capsule. The capsules in the experiments reported here absorbed up to 20 kJ of x rays, about 1/8 of the estimated ignition requirement. It remains to be seen whether adequate symmetry and pulse shaping can be obtained.

Recent work [5,6] demonstrated that the effect of random *Z*-pinch nonuniformities on the shock radiation source was very small. Systematic asymmetries appear to be the most significant issue. The cylindrical ZPDH tends to drive the spherical capsule with equator-hot radiation that, if uncorrected, will produce an implosion elongated along the cylinder axis. Symmetry corrections, including radiation shields, noncylindrical foams, and local foam dopants, require accurate symmetry diagnostics. Prior work [7] showed that symmetry can be inferred from x-ray core imaging measurements of the equatorial plane radius (a) compared to the polar radius (b). Applying this method to the ZPDH is complicated by the difficulty of viewing the implosion through the luminous high-opacity *Z*-pinch plasma (Fig. 1). We used time- and space-resolved x-ray spectra from tracer atoms in the core to ensure that the measurements reflect the core conditions. This requires two separate spectrometers, since each instrument records only 1D spatial information. The equatorial-to-polar radius ratio can be measured using space-direction lineouts from the two spectra. These spectra also lay the foundation for a tomographic reconstruction of the 2D n_e and T_e core spatial profiles. In addition, n_e and T_e measurements benchmark how close the conditions are to ICF requirements and test ZPDH simulation accuracy, since the core conditions depend on the drive radiation.

In this Letter we describe sample results from two experiment groups. The goal for the first group was maximizing the likelihood of measuring core x-ray emission. The experiment representing the first group, Z860, used a 1.7 mm outer diameter capsule with a 36 μm CH wall and a 4 μm polyvinylalcohol (PVA) overcoat to retain the fill gas. The fill was 2.8 atm CD_4 + 0.085 atm Ar. CD_4 was chosen to avoid the difficulty of retaining D_2 in the capsule.

The second experiment group used a larger capsule and a lower-Z fill gas to increase the Ar emission intensity. The experiment representing this second group, Z962, used a capsule with a 2.1 mm diameter, a 39 μm CH wall,

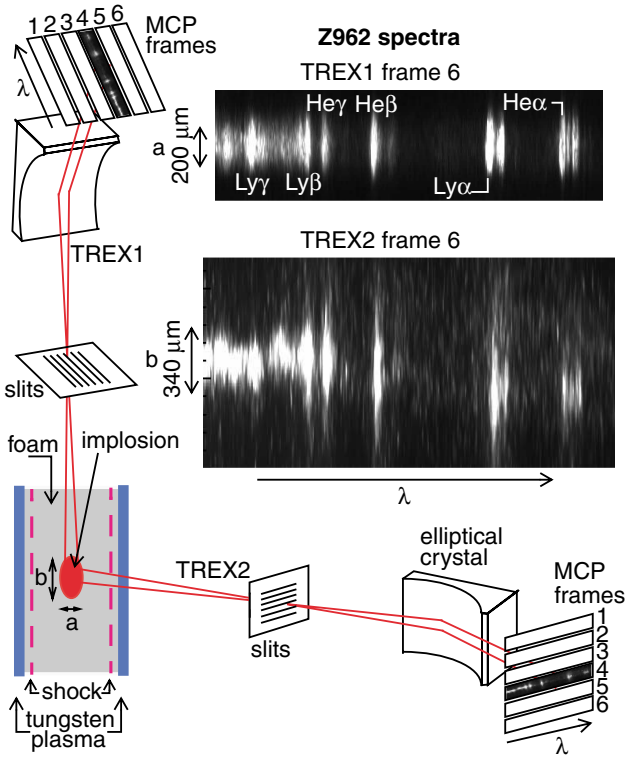

FIG. 1 (color). Schematic experiment diagram. The dynamic hohlraum forms when the tungsten Z-pinch plasma collides with the foam. TREX1 and TREX2 are spectrometers oriented with spatial resolution directions to measure the implosion core size along the equatorial axis (a) and polar axis (b), respectively. The MCP frames record space-resolved spectra at 1 ns time intervals. The Ar spectra were recorded at the peak emission time in experiment Z962.

a 4 μm PVA layer, and an 800 Å Al overcoat. The fill gas was 13.5 atm D_2 + 0.085 atm Ar.

The experiments used the Z facility [2,3] to drive a ZPDH [3,6,8] using a 240-wire 40 mm diameter outer array and a concentric 120-wire 20 mm diameter inner array. The tungsten wire diameter was 7.5 μm. The 14 mg/cc CH_2 foam was 6 mm diameter, 10 mm tall on Z860, and 12 mm tall on Z962. Polar line of sight measurements were performed through a 4 mm diameter aperture that was covered with a 4 μm Ti + 2 μm CH foil to reduce symmetry perturbations. The time-dependent radiation temperature, shock, and capsule radius were diagnosed using x-ray imaging and power measurements [6,8,9]. The ~18 Mbar shock had a ~35 cm/μs velocity and the radiation drive temperature rose over ~7 ns to ~220 eV, prior to the shock arrival on axis. The capsule core x-ray emission peaked 2–3 ns before shock arrival on axis and 4–5 ns prior to Z-pinch stagnation. The times given below are with respect to Z-pinch stagnation [8]. The diagnostic suite [10] included photoconducting diode capsule implosion time measurements and activation and time-of-flight neutron detectors. The neutron yield was ~2×10^{10} on Z962, similar to the 1D simulation yield. The Z860 yield was below the ~3×10^9 detector threshold. Comparisons of measured and simulated neutron yields, ZPDH radiation, and hydrodynamics will be described elsewhere.

Here we emphasize the results from two time- and space-resolved elliptical crystal spectrometers [11] (TREX1 and TREX2). The TREX1 spectrometer viewed the capsule along the polar axis (Fig. 1). It used six slits to project spatially and spectrally resolved capsule images onto six 1 nsec time-gated microchannel plate (MCP) strip lines. On Z860 and Z962 the spatial resolution was ~330 μm and ~120 μm, respectively. The pentaerythritol crystal located 2.92 m from the source provided a 1.3 Å spectral range and a spectral resolution of $\lambda/\delta\lambda \sim 860$. On Z962 the TREX2 spectrometer viewed the capsule from the side. The spectral range and resolution were the same as for TREX1, except that the source to crystal distance was 4.10 m and the spatial resolution was ~200 μm. We account for the relative instrument sensitivity using Ref. [11], as calibrations were unavailable.

On Z860 TREX1 recorded Ar spectra in time frames 1 and 2 (Fig. 2). The emission spatial extent was ~300 μm, demonstrating that the Ar spectra arise from a well-localized implosion core. A time-resolved x-ray pinhole camera [10] image was recorded simultaneously with the TREX1 frame 1 spectrum (Fig. 6 in Ref. [5]). This image confirmed that the implosion was radiation driven, since the shock in the foam was still at a ~1.8 mm diameter.

The TREX1 data (Fig. 2) are qualitatively similar to laser hohlraum implosion data [12]. A "line of best fit" analysis [13] of the Stark- [14] and opacity-broadened He-like and H-like Ar lines was used to determine n_e and the areal density $n_{li}\delta r$, where n_{li} is the lower level population of ion charge state i and δr is the plasma size along the line of sight. The density and areal density uncertainties correspond to the standard deviation of the line of best fit intersection values [13]. T_e was determined from the Lyγ/Heγ and the (He-like satellites to Lyα)/(Li-like satellites to Heα) line intensity ratios, interpreted using the nonlocal thermodynamic equilibrium collisional-radiative SPECT3D model [15]. The model

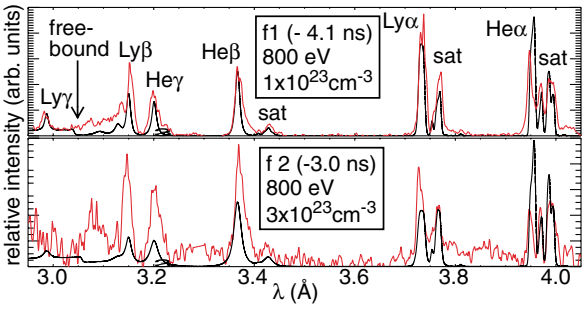

FIG. 2 (color). Spatially averaged TREX1 Ar spectra from Z860. Synthetic spectra (black) calculated with the SPECT3D model at the specified T_e and n_e are superimposed on the data (red). The times are specified with respect to the Z-pinch stagnation.

includes Stark broadening [14,16] and plasma opacity. Our analysis assumed a uniform steady-state Maxwellian plasma. The temperature represents a weighted average of the values inferred from the different line ratios. Typical uncertainties in the measured ratios are ±25%, leading to roughly ±50 eV T_e uncertainty. The total T_e uncertainty includes contributions from the uncertainty in measuring the line intensities, density effects on the line ratios, estimates for the accuracy of the relative instrument efficiency, and estimates for possible atomic model inaccuracies.

The core conditions inferred from the Z860 data are shown in Fig. 3. At −4.1 ns, $\rho \sim 0.42$ g/cm^3 and the ρr obtained from the $n_{li}\delta r$ product was 11 ± 2 mg/cm^2 (assuming the Ar concentration was preserved). The values at −3.0 ns were $\rho \sim 1.07$ g/cm^3 and $\rho r \sim 5 \pm 2$ mg/cm^2. The $n_{li}\delta r$ values lead to Ar line center optical depths of $\tau \sim 50$–100 for Heα and Lyα, $\tau \sim 3$ for Heβ and Lyβ, and $\tau \sim 0.3$–1.0 for the Heγ and Lyγ lines.

As a consistency check the data are compared with synthetic SPECT3D spectra calculated at the inferred T_e, n_e, and ρr values (Fig. 2). The agreement at −4.1 ns shows that the data are consistent with the uniform core approximation. However, at −3.0 ns the high-n lines are not well reproduced. Also, the −3.0 ns spectrum is ∼5× weaker than at −4.1 ns. A preliminary interpretation is that at −3.0 ns a small residual hot core emits the lines through a cool outer layer that has enough ground state Ar population to attenuate the resonance transitions.

An estimate for the radial compression (C_r) can be obtained from the ratio of the compressed core density compared with the initial density and assuming a spherical implosion. The −4.1 and −3.0 ns data correspond to $C_r \sim 5.4$ and $C_r \sim 7.4$, respectively. The actual shape of the implosion is expected to be prolate, since no symmetry corrections were employed here.

The ZPDH properties were calculated [5] with 2D LASNEX [17] simulations that use multigroup diffusion radiation transport, treat the electrodes as a boundary with a specified time-dependent albedo, and treat the capsule as a loss in the central zones. They neglect Rayleigh-Taylor instabilities, an approximation justified by Refs. [5,6,8]. The radiation field at the capsule location was calculated by integrating the radiation transport equation within the ZPDH. This radiation was averaged over the capsule surface and used as input for 1D simulations of the capsule implosion. The simulation implosion core T_e and n_e profiles were postprocessed to obtain values that are spatially averaged and emissivity weighted in a similar manner as for the experiment. The simulation relative timing was established using the measured ZPDH shock trajectory [6]. The simulation n_e and T_e values agree with the experiment at peak core emission intensity. The 0.5 ns timing difference is comparable to the experiment uncertainty. The simulations do not reproduce the residual hot core that is inferred at −3.0 ns, although the n_e rise is very similar to the experiment.

On Z962, spectra were recorded on TREX1 at −6.7, −5.7, and −4.5 ns and on TREX2 at −4.5 ns (Figs. 1 and 4). The TREX1 spectral intensities at −6.7 and −5.7 ns were weaker than the −4.5 ns spectrum by factors of ∼250 and 10, respectively. The weak early signals were not observed on TREX2. The core T_e and n_e were determined from the Fig. 4 data using the methods outlined above (Fig. 3). At −4.5 ns, the time of peak emission, the values were $\rho \sim 0.44$ g/cm^3, $\rho r \sim 8.7 \pm 0.9$ mg/cm^2, and $C_r \sim 5.5$. The postprocessed simulation peak T_e agrees with the data, while n_e is about 0.6 times the experiment value (Fig. 3). The emission peaks approximately 0.5 ns later in the simulation. Also, the data indicate that a relatively small amount of fuel is heated to high temperatures ∼2 ns before the emission peaks, a feature not reproduced in the simulations.

The absorbed x-ray energy in the Z962 simulations was ∼20 kJ, to our knowledge approximately an order of magnitude higher than in prior [1] laser hohlraum implosions. We reiterate that good control over drive

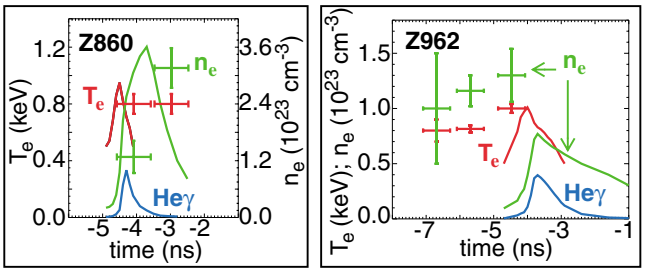

FIG. 3 (color). Time-resolved spatially averaged T_e and n_e measurements (symbols with error bars) compared with postprocessed simulations (solid curves). Red, green, and blue represent T_e, n_e, and Ar Heγ intensity, respectively.

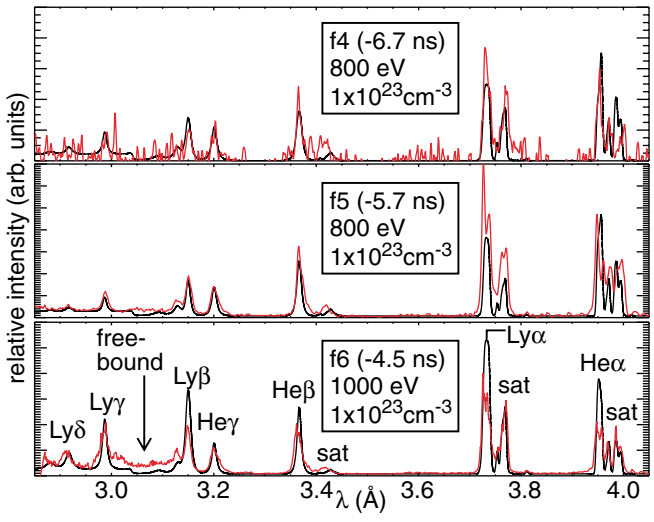

FIG. 4 (color). Spatially averaged TREX1 Ar spectra from Z962. Synthetic spectra (black) calculated with the SPECT3D model at the specified T_e and n_e are superimposed on the data (red).

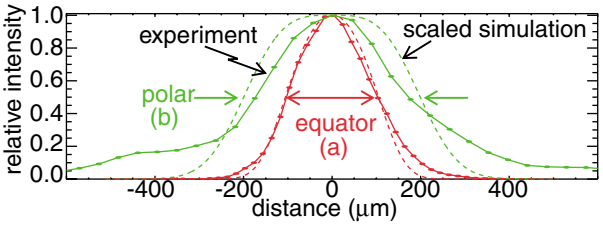

FIG. 5 (color). Space-direction lineouts through the Z962 data (solid lines with symbols). Postprocessed 2D simulation results (dashed lines) are superimposed on the data. The size of the simulation results was scaled down by a factor of 1.2 to match the equatorial plane FWHM measurement.

asymmetries has yet to be demonstrated for ZPDH driven implosions. The drive radiation burns through these relatively thin wall capsules when the capsule has imploded to approximately one-half the initial radius. Thin wall capsules were chosen because they are less sensitive to drive asymmetries, although energy coupling is less efficient than for capsules that remain ablative throughout the drive pulse. The absorbed energy is proportional to the drive temperature at the peak compression. Increasing (decreasing) the drive temperature will tend to make the implosion occur earlier (later), making the calculated absorbed energy insensitive to drive uncertainties. Near term experiments can achieve 2 times higher absorbed energy by increasing the ablator opacity. However, the effectiveness of ICF studies depends on simultaneous symmetry control. If symmetry can be improved, then simulations indicate [18] that high yield ICF implosions could be driven by dynamic hohlraums using a future larger Z pinch facility.

Symmetry estimates can be obtained using space-direction lineouts from the two slit-imaged spectra (Fig. 1). Lineouts taken through the optically thin Ar free-bound continuum between the Lyδ and Lyγ transitions (Fig. 5) were selected because the free-bound continuum clearly represents the conditions within the implosion core and the spectral model embedded within the simulations could be used to reliably interpret the data. Results of 2D implosion simulations postprocessed to account for the slit-imaged experiment geometry and the resolution are superimposed on the measurements. The 2D capsule simulations were driven by the time- and angle-dependent radiation obtained in separate ZPDH simulations [5]. The simulations have a compressed size at peak emission that is larger than the experiment by a factor of $\sim$1.2 (Fig. 5), consistent with the lower simulation electron density. However, the simulation ratio $a/b = 0.53$, in good agreement with the experiment value $a/b = 0.59$ (Fig. 5).

The results demonstrate that the ZPDH can produce diagnosable hot and dense capsule implosions. The large absorbed energy supports the inherent energy efficiency of this approach. Work is in progress to exploit the understanding and the measurement techniques developed here to improve the implosion symmetry and increase the coupled x-ray energy.

We thank the Z accelerator, diagnostics, materials processing, target fabrication, and wire array teams for invaluable and dedicated technical assistance. G. Dunham, G. A. Rochau, and L. P. Mix provided data processing assistance. A General Atomics Inc. team led by D. Steinman fabricated the capsules. We are also grateful to R. J. Leeper, J. L. Porter, and M. K. Matzen for support and encouragement. Sandia is a multiprogram laboratory operated by Sandia Corporation, a Lockheed Martin Company, for the U.S. Department of Energy under Contract No. DE-AC04-94AL85000.

[1] J. Lindl, Phys. Plasmas **2**, 3933 (1995).
[2] M.K. Matzen, Phys. Plasmas **4**, 1519 (1997); V. P. Smirnov, Plasma Phys. Controlled Fusion **33**, 1697 (1991); J. H. Brownell, R. L. Bowers, K. D. McLenthan, and D. L. Peterson, Phys. Plasmas **5**, 2071 (1998).
[3] R. J. Leeper *et al.*, Nucl. Fusion **39**, 1283 (1999); T. J. Nash *et al.*, Phys. Plasmas **6**, 2023 (1999).
[4] D. L. Peterson *et al.*, Phys. Plasmas **6**, 2178 (1999); S. A. Slutz *et al.*, Phys. Plasmas **8**, 1673 (2001); J. Lash *et al.*, in *Proceedings of Inertial Fusion Science and Applications 99, Bordeaux, France, 1999*, edited by C. Labaune, W. J. Hogan, and K. A. Tanaka (Elsevier, Paris, 2000), Vol. I, p. 583.
[5] S. A. Slutz *et al.*, Phys. Plasmas **10**, 1875 (2003).
[6] J. E. Bailey *et al.*, Phys. Rev. Lett. **89**, 095004 (2002).
[7] A. Hauer *et al.*, Rev. Sci. Instrum. **66**, 672 (1995).
[8] T.W. L. Sanford *et al.*, Phys. Plasmas **7**, 4669 (2000); T.W. L. Sanford *et al.*, Phys. Plasmas **9**, 3573 (2002).
[9] T. J. Nash *et al.*, Rev. Sci. Instrum. **74**, 2211 (2003).
[10] T. J. Nash *et al.*, Rev. Sci. Instrum. **72**, 1167 (2001).
[11] B. L. Henke, H.T. Yamada, and T. J. Tanaka, Rev. Sci. Instrum. **54**, 1311 (1983); B. L. Henke (private communication).
[12] B. A. Hammel, C. J. Keane, M. D. Cable, D. R. Kania, J. D. Kilkenny, R.W. Lee, and R. Pasha, Phys. Rev. Lett. **70**, 1263 (1993).
[13] J. D. Kilkenny, R.W. Lee, M. H. Key, and J. G. Lunney, Phys. Rev. A **22**, 2746 (1980).
[14] L. A. Woltz and C. F. Hooper, Jr., Phys. Rev. A **38**, 4766 (1988); R. C. Mancini, D. P. Kilcrease, L. A. Woltz, and C. F. Hooper, Jr., Comput. Phys. Commun. **63**, 314 (1991).
[15] J. J. MacFarlane, P. R. Woodruff, and I. E. Golovkin, "SPECT3D Imaging and Spectral Analysis Suite," Prism Computational Sciences Report No. PCS-R-045, 2003, Madison, WI 53711 (unpublished).
[16] D. A. Haynes, D. T. Garber, C. F. Hooper, Jr., R. C. Mancini, Y. T. Lee, D. K. Bradley, J. Delletrez, R. Epstein, and P. Jaanimagi, Phys. Rev. E **53**, 1042 (1996).
[17] G. Zimmerman and W. Kruer, Comments Plasma Phys. Control. Fusion **2**, 85 (1975).
[18] J. S. Lash *et al.*, C. R. Acad. Sci. Paris, Ser. IV **1**, 759 (2000).